JOPSS
JAEA Originated Papers Searching System

日本原子力研究開発機構機関リポジトリ
Japan Atomic Energy Agency Institutional Repository

Title	Cavitation damage in double-walled mercury target vessel
Author(s)	Naoe Takashi, Wakui Takashi, Kinoshita Hidetaka, Kogawa Hiroyuki, Haga Katsuhiro, Harada Masahide, Takada Hiroshi, Futakawa Masatoshi
Citation	Journal of Nuclear Materials,506,p.35-42
Text Version	Accepted Manuscript
URL	https://jopss.jaea.go.jp/search/servlet/search?5057149
DOI	https://doi.org/10.1016/j.jnucmat.2017.10.044
Right	©2017 Elsevier B.V.

Japan Atomic Energy Agency

Cavitation damage in double-walled mercury target vessel

Takashi Naoe[a], Takashi Wakui[a], Hidetaka Kinoshita[a], Hiroyuki Kogawa[a], Katsuhiro Haga[a], Masahide Harada[a], Hiroshi Takada[a], Masatoshi Futakawa[a]

[a] *Japan Atomic Energy Agency, Tokai-mura, Naka-gun, Ibaraki 319-1195, Japan.*

Abstract

A liquid mercury target is operated as part of a spallation neutron source at the Japan Proton Accelerator Research Complex (J-PARC). The mercury target vessel is made of 316L stainless steel, (3 mm thick) and its beam window is damaged by cavitation due to pressure waves in mercury. To mitigate the pressure waves and the cavitation damage, a double-walled structure with a narrow channel of 2 mm was added to the beam window along with gas microbubbles injection technology. After operation of up to 670 MWh for 1670 hours, the beam window of the used target vessel was cut out using an annular cutter to investigate the effect of the double-walled structure on mitigating cavitation damage. Band-like damage distribution due to cavitation was observed on the outer wall that faced the narrow channel, where the maximum pit depth was estimated to be 25 μm. Furthermore, to clarify the mechanisms possibly contributing to the band-like damage distribution, numerical simulations were conducted in terms of flow velocity, gap width, and pressure waves in the narrow channel. The results show that the distribution of accumulated saturation time of negative pressure period obtained from FEM

Email address: naoe.takashi@jaea.go.jp (Takashi Naoe)

simulation correlated well with the experimentally observed band-like damage distribution.
Keywords: Mercury target, Pressure wave, Cavitation damage, Narrow channel, Post irradiation examination

1. Introduction

Liquid mercury target systems have been operated in the spallation neutron source at the Japan Proton Accelerator Research Complex (J-PARC) and the Spallation Neutron Source (SNS) at Oak Ridge National Laboratory (ORNL) to provide intense pulsed proton beams for developing innovative materials and life science research [**?** **?**]. The beam power goal for the J-PARC neutron source is 1 MW at 25 Hz with 1 μs pulse duration. At the moment of proton beam injection into the mercury, pressure waves are generated owing to abrupt heat deposition in mercury, and these waves induce cavitation at the interface between the mercury and the enclosure vessel made of type 316L stainless steel, the so-called target vessel [**?**]. This cavitation causes severe erosion damage at the beam entrance region of the target vessel wall, also called beam window. The cavitation-induced erosion rate is likely to increase with proton beam power. The thickness of the beam window of the target vessel was 3 mm to reduce thermal stress. The structural integrity of the target vessel decreases drastically owing to the cavitation erosion [**?**]. In recent years, post irradiation examinations of used target vessels were performed at the SNS and J-PARC, and cavitation damage was observed at the beam window: the damage penetrated through the inner wall (3 mm thick) of the double-walled SNS target operated up to 3055 MWh (379 MW average power) [**?**], and the maximum depth of 250 μm was observed in case of the J-

PARC neutron target vessel operated up to 475 MWh (128 kW average power) [**?**].

The injection of gas microbubbles into flowing mercury is one of the prospective techniques to mitigate the pressure waves that cause cavitation [**?**]. At J-PARC, a gas microbubble generator for injecting helium gas microbubbles measuring less than 50 μm in radius was developed to mitigate pressure waves and their propagation [**?**]. It was installed in the mercury target system along with the closed gas circulation system in October 2012, and pressure wave mitigation was confirmed by means of vibration measurement of the target vessel [**? ?**]. The previously mentioned target, in which a damage depth of 250 μm was observed, was operated without gas microbubbles injection.

To mitigate the growth of cavitation bubbles by increasing flow velocity, a double-walled structure at the beam window of the target vessel contributing to a narrow mercury flow channel was adopted in addition to gas microbubble injection. It was reported that the mercury flow deforms the growth and collapse of cavitation bubbles and reduces cavitation damage [**?**], and the damage tends to decrease with increasing flow velocity [**?**]. The double-walled target vessel, target No. 5 in terms of fabrication number, was operated from October 2013 to May 2014; the resulting accumulated beam energy was approximately 680 MWhr for 1671 hours of operation. Operation of the double-walled target was terminated owing to failure of the water shroud. Before replacing the target vessel, samples were cut from the beam window to examine the cavitation damage inside the target vessel. In this study, the cavitation damage on samples from the beam window was observed, and the damage depth was measured quantitatively with a surface replication method. Furthermore, the relationship between the damage

distribution and the saturation time related to negative pressure [**?** **?**], which was estimated from numerical simulation, was investigated.

2. Damage inspection of target vessel

2.1. Beam window cutting

A schematic drawing of the double-walled mercury target vessel is shown in Fig. 1. The beam window of the target vessel is composed of a double-walled (inner/outer wall) mercury vessel and a double-walled water shroud. The thickness of the mercury vessel inner wall is 5 mm and that of the other walls is 3 mm. The gap of the narrow channel is set to 2 mm to achieve a mercury flow velocity of approximately 4.0 m/s. The gap width used in the target was based on the results of off-beam cavitation damage experiments in stagnant mercury, which demonstrated that a narrower gap is likely to reduce cavitation damage because the direction of ejection of the micro-jet changes due to the interference of the wall boundary [**?**].

The target beam window was sampled using an annular cutter without any lubricant by using the same procedure as that described in Refs. [**?** **?**]. For target No. 5, it was necessary to cut through four layers of 316L SS to inspect the innermost wall of the mercury vessel. A photograph of target vessel cutting is shown in Fig. 2(a). Figs. 2 (b) and (c) show photographs of the annular cutter before and after cutting. The cutter teeth broke due to the stress imposed during cutting operation, and heat was generated owing to the cutter body rubbing on the target after the teeth were damaged. Because the replacement cutters continued to break, we stopped sampling of the mercury vessel inner wall.

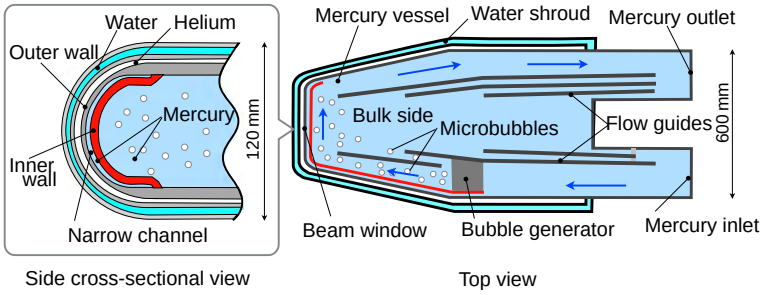

Fig. 1. Schematic of double-walled mercury target vessel at J-PARC with gas microbubble generator. (Target No. 5)

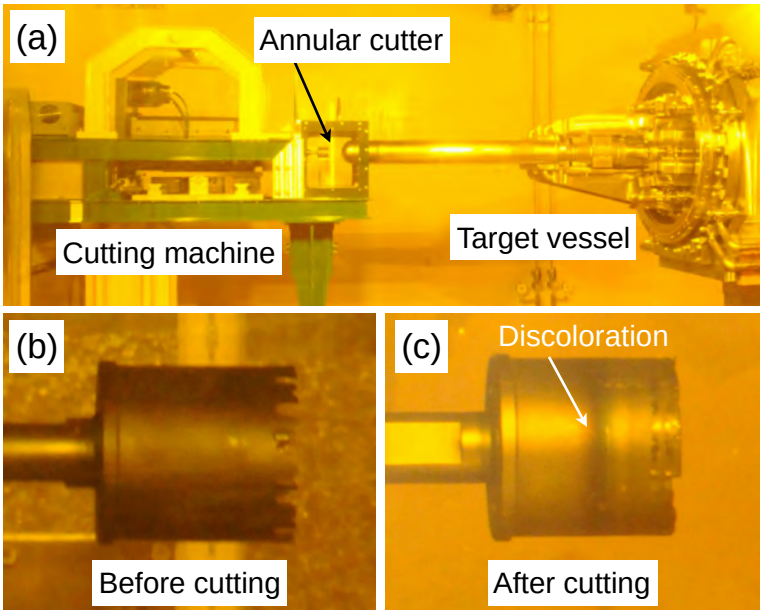

Fig. 2. Photographs of (a) target vessel cutting machine, annular cutters (b) before and (c) after cutting.

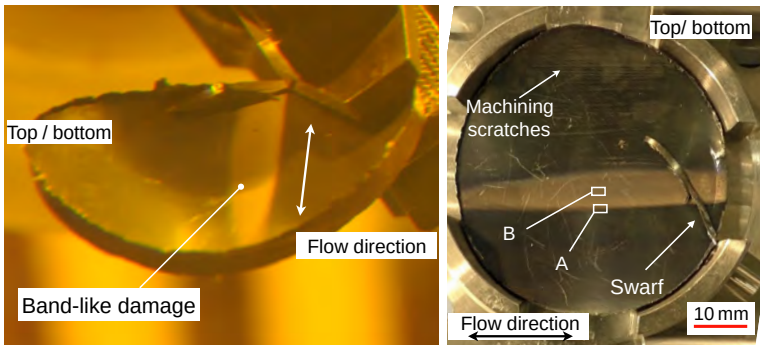

Fig. 3. Photographs of specimen from mercury vessel outer wall.

2.2. Visual inspection

The specimens cut out from the outer/inner water shrouds walls and the outer wall of mercury vessel were washed in an ultrasonic water bath for 60 min to remove mercury and spallation products. No visible damage was observed on the surface of the outer/inner water shrouds facing the water. Fig. 3 shows photographs of the specimen cut from the mercury vessel outer wall. The orientation of target vessel (top/bottom) on the specimen is unknown. The band-like damage occurred parallel to the flow direction. Machining scratches suggesting non-severe damage compared to the damage to the center part are present on the top/bottom side. The inner wall surface observed through the cutting hole is shown in Fig. 4. No visible damage could be observed, except for machining scratches on the surface, although surface discoloration was observed. The mitigating effect of bubble injection on cavitation damage was not confirmed because the inner wall specimen was not cut from the mercury vessel.

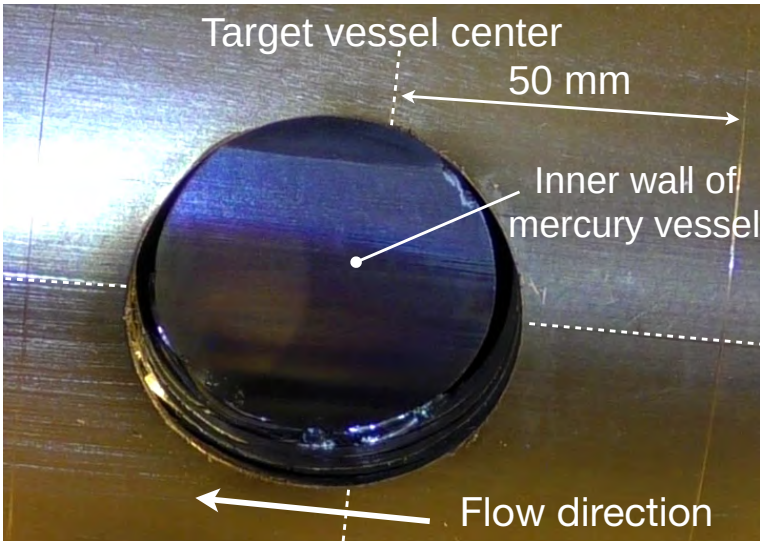

Fig. 4. Photographs of beam window of target vessel after cutting.

2.3. Damage evaluation

To quantitatively evaluate the cavitation damage to the narrow channel surface, a silicone rubber surface replica (Struers, Repliset-F1) was used to measure the surface roughness of the specimens. Hands on analysis of the specimen was not possible because it had a high-dose rate of 55 Sv/h at contact. After replicating the specimen surface, the replica was sealed using an airtight-cell with a transparent glass window measuring 0.5 mm in thickness. The replicated surface was observed quantitatively through the glass window by using a laser scanning microscope (LSM) (Keyence, VK-9510). To evaluate the mean depth of erosion, the vertically jointed depth contour of the replicated band-like damage was measured. Fig. 5(a) shows the jointed image of the replicated surface of the mercury vessel outer wall. Machining scratches can be seen near the I and IV positions. Furthermore, the number density of pits seems to increase gradually toward the

center of the band-like damage. Figs. 5(b) and (c) shows the depth profiles of the replicated surface for sections I–IV and the curvature corrected depth profile with smoothing line, respectively. Here, the curvature was corrected by assuming R=43.2 mm to fit the shape around both edges. Thickness reduction due to cavitation erosion was not detected, because undulations in the corrected profile with smoothing line (±10 μm) were larger than homogeneous erosion.

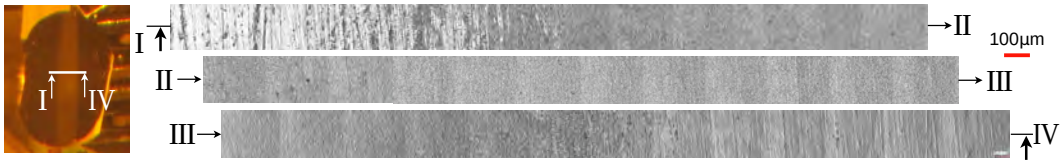

(a) Confocal images of replicated surface

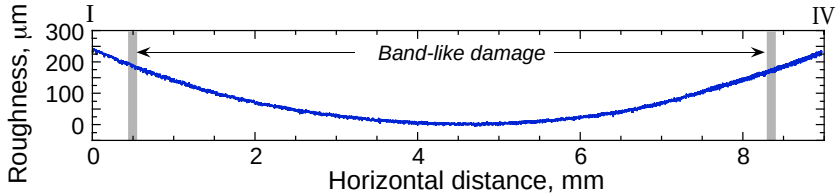

(b) Depth profile of sections I–IV

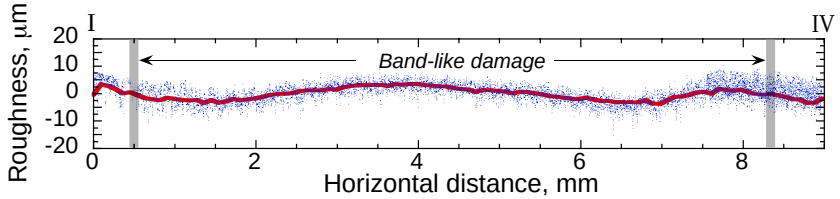

(c) Curvature corrected depth profile of sections I–IV

Fig. 5. Confocal image and depth profiles of band like damage.

Fig. 6 shows high-magnification confocal images and depth profiles obtained using the LSM. The replicated locations—**A** for boundary of band-like damage, **B** for center of band-like damage—are marked in Fig. 3. The machined scratches

remained outside of the area with band-like damage (Field (2)). At around the boundary of the band-like damage (Fields (1) and (3)), multiple isolated pits, which are thought to be formed mainly by cavitation, are distributed, and the number of pits increases toward the center of the band-like damage. Therefore, it is thought that the band-like damage was formed by the accumulation of pits due to cavitation. At around the center of the band-like damage (Fields B and (4)), relatively deep pits are distributed upon the accumulated pits. The measured maximum pit depth is approximately 25 μm, which is slightly deeper than the predicted damage depth of 10~15 μm based on the prediction method proposed in the previous study [**?**]. Surface roughness R_a at around the boundary of the band-like damage a–a', and b–b', and that around the center c–c' were 2.27 μm, 4.37 μm, and 4.30 μm, respectively.

3. Discussion

Based on an inspection of the mercury vessel outer wall facing the narrow channel, the presence of band-like damage distribution parallel to the mercury flow direction was confirmed. By contrast, in case of the SNS mercury target vessel, which had a double-walled structure since initial operation, band-like damage in the narrow channel was less noticeable despite the duration of operation and proton beam power being longer and higher, respectively, than those in J-PARC [**? ?**]. To understand the cause of the band-like damage distribution, several factors were investigated. The possible influencing factors are distributions of narrow channel gap width, mercury flow velocity distribution in the narrow channel, and negative pressure distributions.

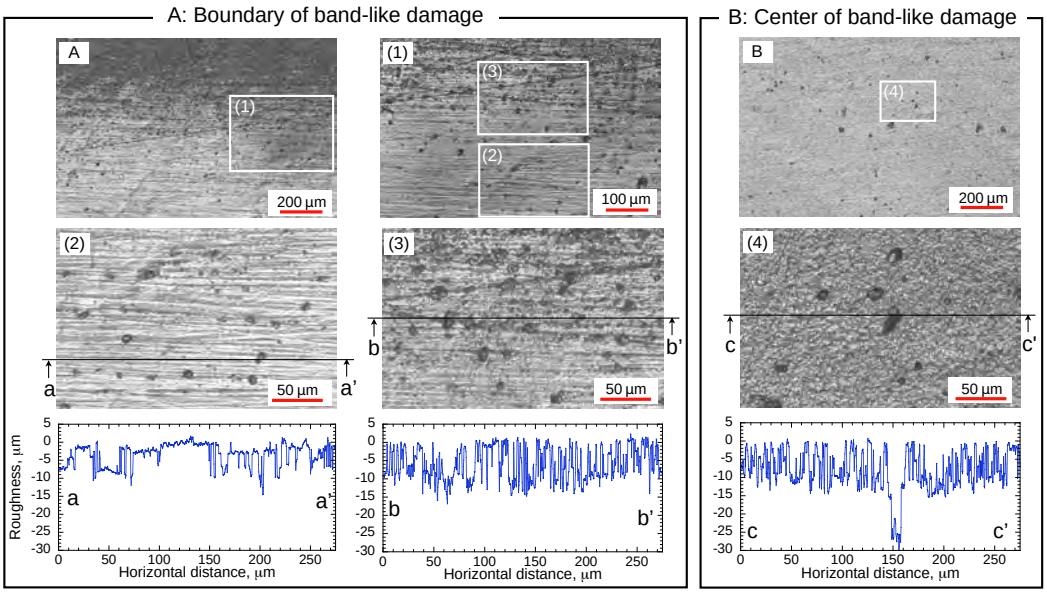

Fig. 6. Confocal images and depth profiles of outer wall of mercury vessel. A and B denote the replicated locations marked in Fig. 3.

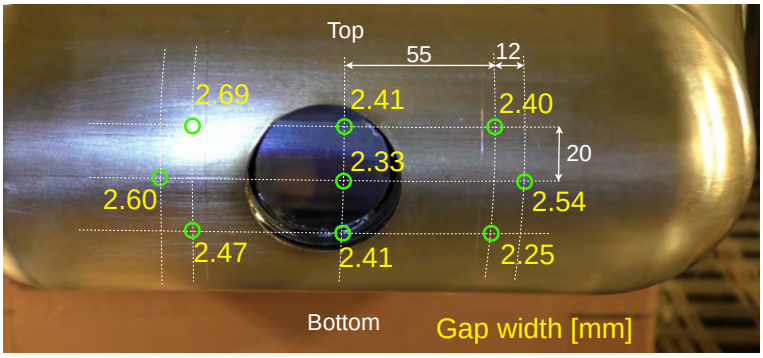

Fig. 7. Gap width of narrow channel obtained from fabrication inspection.

3.1. Effect of gap width

Fig. 7 shows the gap width of the narrow channel measured at the time of fabrication inspection. The gap widths were measured at three heights on the vessel: bottom, center, and top. In a previous study, cavitation damage in a narrow channel was investigated by changing gap widths under a stagnant flow condition during off-beam experiments [**?**]. The results showed that pressure-wave-induced cavitation damage decreased with decreasing gap width. At the cut-out location on the target vessel, the gap width at the center is narrower compared to that at the top and the bottom sides, and more damage was observed at the center relative to the top and the bottom sides. Thus, gap width distribution is thought to not influence the band-like damage distribution.

3.2. Flow velocity distribution

Mercury flow velocity distribution in the narrow channel was investigated using ANSYS FLUENT [**?**] simulation software. Fig. 8 shows the flow velocity distribution at the center of the narrow channel in the vertical plane for gap widths of 1 mm and 2 mm. Inlet flow velocity in the mercury piping of the target vessel

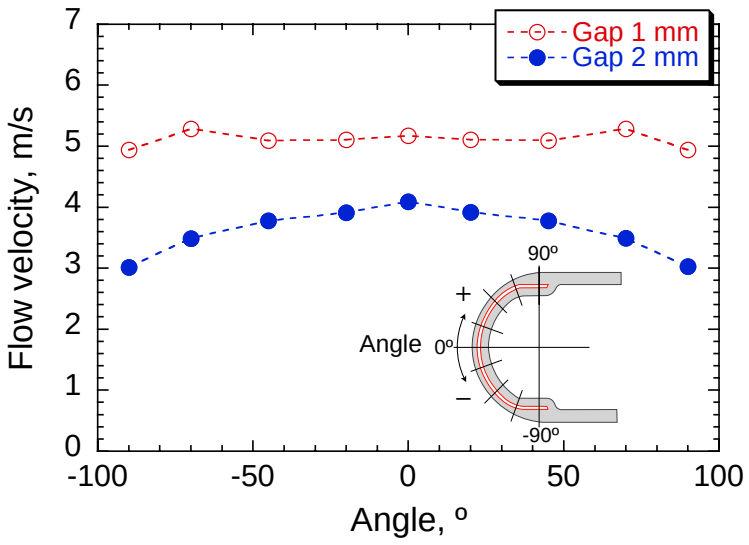

Fig. 8. Flow velocity distribution in narrow channel for gap widths of 1 mm and 2 mm [**?**].

was set to 1.025 m/s based on the rated flow rate of the J-PARC mercury target (34.6 m^3/h). More detailed information on the numerical simulation can be found in Ref. [**?**]. The flow velocity around the center (0°) is similar to the flow velocity at the top and bottom sides of the cutout specimen (±20°), regardless of gap width. In off-beam and on-beam cavitation damage experiments, it has been found that cavitation damage decreases with increasing mercury flow velocity [**? ?**]. Thus, it is difficult to correlate the band-like damage distribution and the flow velocity distribution.

3.3. Negative pressure distribution

3.3.1. Calculation model and condition

To evaluate the negative pressure distribution in the narrow channel, pressure wave propagation in the mercury vessel was evaluated using the conventional finite element method (FEM) code LS-DYNA [**?**]. It is known that cavitation bubbles keep growing under negative pressures lower than the Blake threshold, which is the critical pressure for bubble growth, and they collapse when the pressure rises beyond said level [**?**]. It has been reported that the saturation time of negative pressure, which is the interval between the start and end of negative pressure saturation at the threshold (cut-off pressure in simulation), the so-called negative pressure period, is correlated to the cavitation bubble radius, and the expansion ratio of cavitation bubbles is correlated to the cavitation intensity in damage formation [**?** **?**]. It was confirmed from previous observations that the distribution of cavitation damage inside the mercury target vessels of the SNS and the J-PARC is well correlated with the numerically estimated distribution of the negative pressure period [**?** **?**].

Fig. 9 shows the FEM model of the double-walled mercury target vessel. Hexahedral meshes measuring $1.5 \times 2.0 \times 0.6$ mm in the minimum element size, were used in the model. The total numbers of nodes and elements were approximately 5 million and 4.5 million, respectively. The cut-off pressure due to cavitation was assumed to be -0.15 MPa in mercury, which was estimated on the basis of a comparison of the analytical and experimental results of experiments performed at the LANSCE-WNR facility [**?**]. The pressure response time histories and their distribution in mercury were calculated. Pressure distribution based on nuclear heating calculations by usingthe PHITS code with the JENDEL library [**?** **?**],

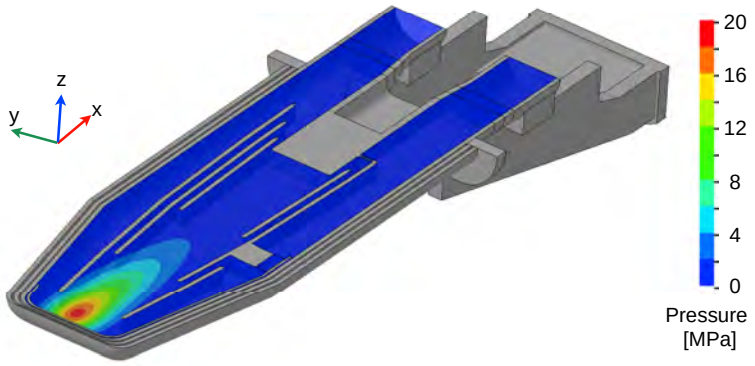

Fig. 9. FEM model and initial pressure distribution for simulating pressure wave propagation.

as shown in Fig. 9, was used as the initial simulation conditions. The beam condition for peak heat deposition in mercury was 500 kW with a Gaussian beam profile of 190 W/cm^3 (7.6 J/cc/pulse), which was the highest beam power for the target operation. Details are given in Appendix A. The maximum initial pressure in mercury was 18.8 MPa on the bulk side. It should be noted that the FEM simulation of pressure wave propagation used in this study excluded the effect of gas microbubbles injection. In this study, for simplified analysis, we assumed that the gas microbubble effect is equivalent to the reduction of proton beam power.

3.3.2. Distribution of negative pressure period

To investigate the distribution of negative pressure period, the accumulated saturation time of negative pressure was defined as follows:

$$T_{N_{accum}} = \sum_{i=1}^{n} T_{N_i} \tag{1}$$

where T_N is the duration for which the pressure exceeded −0.15 MPa with a calculation interval of 10 μs, and i is the frequency of pressure exceeding −0.15 MPa within the calculation time t. Fig. 10 shows the distributions of $T_{N_{accum}}$ at the outer and the inner walls facing the narrow channel for different calculation times. The $T_{N_{accum}}$ distribution is asymmetric because of the geometry of narrow channel, regardless of the calculation time. For the mercury vessel outer wall, negative pressure period at the center is relatively longer compared to the top and bottom sides of the cut location (marked with a white circle in the figure). This pattern is correlated to the band-like damage distribution shown in Fig. 3. By contrast, in case of the inner wall facing the narrow channel, the distribution of $T_{N_{accum}}$ is band-like, but no damage distributions were recognized during visual inspection, as shown in Fig. 4.

In addition to the center area, relatively long $T_{N_{accum}}$ was calculated along the outer and the inner walls on opposite side of the bubble generator.

3.3.3. Cavitation bubble behavior in narrow channel

Fig. 11(a) shows the time responses of mercury pressure obtained from FEM simulation at the center of the outer and the inner wall surfaces at 500 kW. At the center, the pressure difference between the outer wall and the inner wall is barely noticeable. The peak pressure of 14.2 MPa at the inner wall surface is present at the initial state, and then, the pressure decreases to −0.15 MPa (cut-off pressure) and saturates until around 1 ms. After 3 ms, the pressure frequently reaches the cut-off pressure, but each of the saturation times is shorter than that observed during the early stage.

To investigate cavitation bubble behavior in the narrow channel, time responses of cavitation bubbles were calculated using the Keller equation which is the equa-

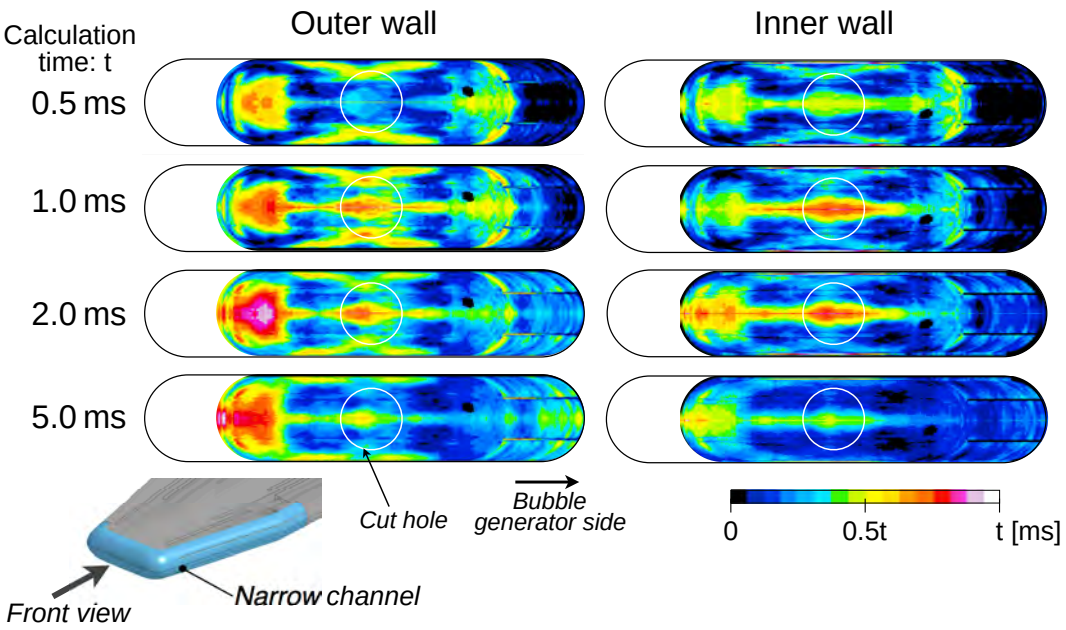

Fig. 10. Distribution of accumulated time of negative pressure period, $T_{N_{accm}}$, for mercury vessel outer and inner walls.

tion of motion for a single bubble in a compressive fluid [**?** **?**]. The time-dependent bubble radius was calculated with assumptions of a spherical single bubble with a 20 μm initial radius and stagnant flow condition. Note that the calculation did not consider the effect of injected gas microbubbles. An explanation of the calculation is given in Appendix B. Fig. 11(b) shows the cavitation bubble response to the pressure waves in the narrow channel shown in Fig. 11(a). Although this calculation excludes the wall boundary effect, cavitation bubbles can come into contact with the narrow channel walls at 500 kW. It has been reported that the ejection direction of the micro-jet, which is emitted during cavitation bubble collapse and causes cavitation damage, changes depending on the distance from the wall surface and the ratio of bubble size to the gap width [**?** **?**]. Consequently, in the case of a bubble in contact with two walls, the micro-jet is ejected parallel to the wall. Thus, cavitation damage might be less than that in the case of no contact with the wall structure.

Fig. 11(c) and (d) shows the pressure and cavitation bubble responses to a beam power of 300 kW, where the pressure waves were assumed to be reduced by injecting gas microbubbles on the mercury bulk side. In the case of 300 kW, the cavitation bubbles are not in contact with the wall. Therefore, the direction of ejection of the micro-jet might be perpendicular to the wall and may lead to more severe cavitation damage than that at 500 kW.

At the off-center location downstream of the narrow channel, simulation indicates relatively longer $T_{N_{accum}}$ distribution than that at the center due to repeated occurrence of short negative pressure periods, as shown in Fig. 10. It is necessary to maintain attention on the damage at the off-center location, although the cutting at the off-center location was not performed in this study because it was reported

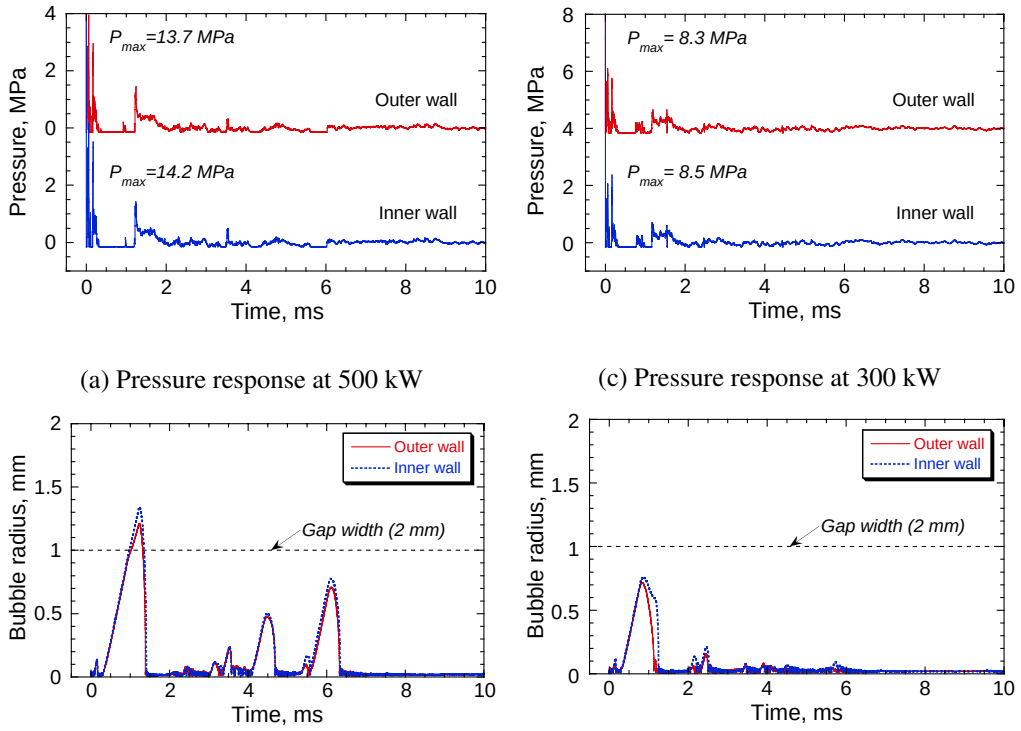

(a) Pressure response at 500 kW

(c) Pressure response at 300 kW

(b) Cavitation bubble response at 500 kW

(d) Cavitation bubble response at 300 kW

Fig. 11. Time histories of pressure and cavitation bubble behavior in narrow channel.

that severe damage was observed at an off-center region in the SNS target vessel, where the negative pressure period was relatively longer compared to that at the target center [**?**].

Furthermore, it was reported that the collapse direction of cavitation bubbles (ejection direction of the micro-jet) depends on the ratio of gap width to bubble radius when cavitation growth and collapse occurs near a wall [**?**]. This is likely why the damage was observed only on the outer wall surface.

4. Conclusion

A mercury target vessel with the double-walled structure was operated at the pulsed spallation neutron source at J-PARC. After operation to a total energy of 680 MWh (406 kW average power), a sample from the beam window was inspected for indications of cavitation damage.

The inspections showed that band-like erosion damage was formed on the outer wall of the mercury vessel surface facing the narrow channel. A maximum erosion depth of approximately 25 μm was measured near the outer wall sample center, whereas no visible cavitation damage was observed on the inner wall surface facing the narrow channel.

To investigate the factors that may influence the formation of band-like damage, numerical simulations were carried out to better understand the influence of the gap width, flow velocity distributions, and negative pressure in the narrow channel. The flow simulation results showed that the flow velocity distribution around the center of the narrow channel was almost uniform, and the results of damage experiments under flowing conditions suggest the flow velocity was unlikely to cause band-like damage. The pressure wave simulation results showed

that the distribution in the accumulated saturation time of negative pressure, which was defined as the negative pressure period, correlated well with the observed damage distribution.

Appendix A. Heat deposition distribution for mercury target

To calculate the pressure time response in the mercury, heat deposition distribution is needed as input data. The heat deposition distribution for the J-PARC Gaussian beam profile under the 1 MW condition is expressed as follows:

$$q(x,y,z) = f_a(x)\exp\left(-\frac{y^{f_d(x)}}{f_b(x)^2} - \frac{z^{f_e(x)}}{f_c(x)^2}\right) + f_f(x) \quad (x < 40\ cm) \tag{A.1}$$

where x, y, and z cm are the coordinates of the proton beam direction, and horizontal, and vertical directions, respectively. The coordinate origin is the center of the neutron source, for example, the center of the beam window facing mercury is $(x, y, z) = (-16.65, 0, 0)$. The fitting functions from f_a to f_f are as follows:

$$\begin{aligned} f_a(x) &= A_0 + A_1 x + A_2 x^2 + \ldots + A_8 x^8 \\ &\vdots \\ f_f(x) &= F_0 + F_1 x + F_2 x^2 + F_3 x^3 + F_4 x^4 \end{aligned} \tag{A.2}$$

where A_0 to F_4 are constants given in Table A.1. For the beam power of 500 kW, heat deposition was scaled uniformly to half of that under the 1 MW condition. Fig. A.12 shows the heat deposition distributions in the proton beam direction ($y = z = 0$), horizontal direction ($x = -13.65$ cm, $z = 0$), and vertical direction ($x = -13.65$ cm, $y = 0$) under the 500 kW condition, and these were used for the pressure wave simulation in this study. From the heat deposition distribution, the

initial pressure distribution used for the input of FEM simulation was calculated as follows [**?**]:

$$P(x, y, z) = K\beta\Delta T(x, y, z) = K\beta\frac{q(x, y, z)}{25C_p\rho} \tag{A.3}$$

where $K = 25.6$ GPa is the bulk modulus, $\beta = 1.81 \times 10^{-4}$ 1/K is the expansion rate, ΔT is the temperature rise, $C_p = 139$ J/kg·K is the specific heat of mercury under constant pressure, and $\rho = 13528$ kg/m^3 is the density. It is noted that the 25 1/s denotes the conversion factor for the heat deposition from W/cm^3 to the energy deposition J/cm^3 at 25 Hz.

TableA.1. Fitting parameters for Eq. (A.2)

	A	B	C	D	E	F
0	2.0541×10^{2}	6.2435×10^{0}	2.7660×10^{0}	2.1186×10^{0}	1.7789×10^{0}	8.0911×10^{0}
1	-1.1667×10^{1}	1.3976×10^{-2}	1.7757×10^{-2}	-9.8580×10^{-4}	-6.0138×10^{-3}	-2.9959×10^{-2}
2	2.8801×10^{-1}	-9.7951×10^{-4}	7.7297×10^{-4}	-1.4036×10^{-4}	6.0685×10^{-4}	-1.6117×10^{-2}
3	-1.5619×10^{-2}	2.9654×10^{-5}	-1.4558×10^{-5}	3.9033×10^{-6}	-1.2978×10^{-5}	6.0189×10^{-4}
4	2.4702×10^{-4}					-7.0140×10^{-6}
5	8.6179×10^{-5}					
6	-5.8780×10^{-6}					
7	1.4210×10^{-7}					
8	-1.1984×10^{-9}					

Appendix B. Calculation of single cavitation bubble behavior

The cavitation bubble behavior was calculated using the Keller equation [**?** **?**] with the assumption of a spherical bubble in compressible liquid as follows [**?**]:

$$\left(1 - \frac{\dot{R}}{C_L}\right)R\ddot{R} + \left(\frac{3}{2} - \frac{\dot{R}}{2C_L}\right)\dot{R}^2 = \frac{1}{\rho}\left(1 + \frac{\dot{R}}{C_L}\right)(P_b[t] - P_{ex}[t + R/C_L] - P_0) + \frac{R}{\rho C_L}\dot{P}_b[t] \tag{B.1}$$

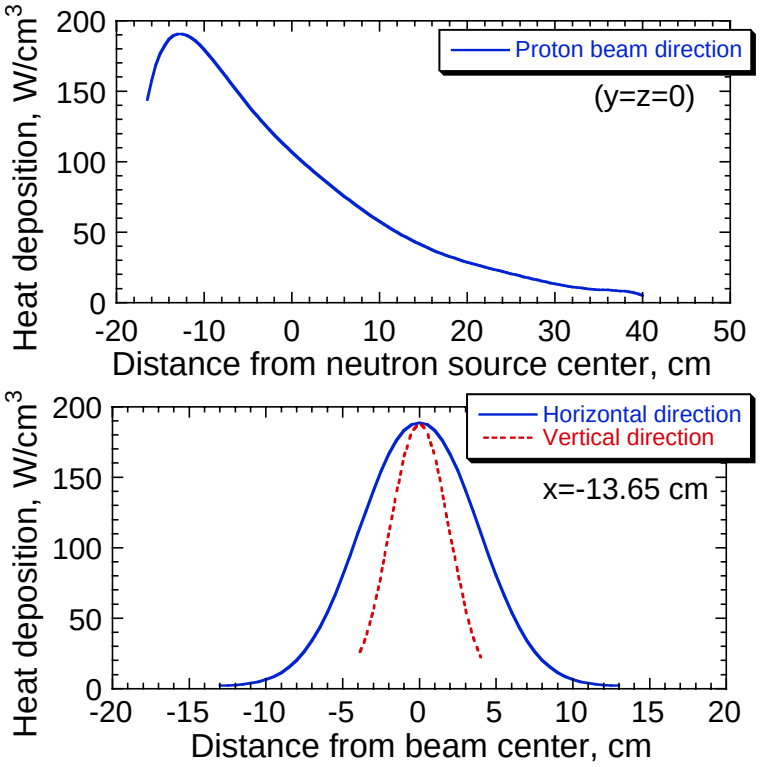

Fig. A.12. Heat deposition distribution in mercury along proton beam direction ($y = z = 0$), horizontal direction ($x = -13.65$ cm, $z = 0$), and vertical direction ($x = -13.65$ cm, $y = 0$) under the 500 kW condition

where $R = R[t]$ is the time-dependent bubble radius, R_0 is the core of cavitation bubble radius ($R_0 = 20$ μm was used in this study), C_L is the speed of sound in liquid, ρ is the liquid density, P_{ex} is the time-dependent external pressure obtained in the FEM simulation, P_0 is the initial pressure, and the overdots are time derivatives. P_b and P_g are the liquid-side and gas-side pressures of the bubble interface as follows:

$$P_b[t] = P_g[t] - \frac{2\sigma + 4\eta\dot{R}[t]}{R[t]}, \tag{B.2}$$

$$P_g[t] = \left(P_0 - P_V + \frac{2\sigma}{R[t]}\right)\left(\frac{R_0}{R[t]}\right)^{3\kappa} + P_V \tag{B.3}$$

where σ is the surface tension, η the viscosity, P_V the vapor pressure, and κ the specific heat ratio. The liquid properties of the mercury used in this study are as follows: $C_L = 1450$ m/s, $\rho = 13528$ kg/m^3, $P_V = 0.28$ Pa, $\sigma = 0.47$ N/m, $\eta = 1.52 \times 10^{-3}$ Pa·s, $\kappa = 1.402$, and $P_0 = 0.103$ MPa.

Acknowledgments

The authors thank Messrs. Norio Narui, Kohei Hanano, Masakazu Seki, Hideki Ueno, and Mitsunori Hirane of JAEA for their assistance with the remote handling tools during cutting and inspection of the target vessel. We are also indebted to Dr. Tetsuya Kai and Mr. Toshiji Uchida of JAEA with their help for the radioactive gas control and an off-gas process system. Furthermore, we are grateful to the members of the Neutron Source Section and Radiation Safety Section of J-PARC Center of JAEA for their support and advice on this work.